

Seismic Reliability Assessment of Typical Road Bridges in Hungary

József Simon & László Gergely Vigh

To cite this article: József Simon & László Gergely Vigh (2017): Seismic Reliability Assessment of Typical Road Bridges in Hungary, Journal of Earthquake Engineering, DOI: [10.1080/13632469.2017.1297270](https://doi.org/10.1080/13632469.2017.1297270)

To link to this article: <http://dx.doi.org/10.1080/13632469.2017.1297270>



Published online: 12 May 2017.



Submit your article to this journal [↗](#)




View related articles [↗](#)



View Crossmark data [↗](#)



Seismic Reliability Assessment of Typical Road Bridges in Hungary

József Simon  and László Gergely Vigh

Department of Structural Engineering, Budapest University of Technology and Economics, Budapest, Hungary

ABSTRACT

Prior to modern seismic codes, several road bridges were not designed for earthquakes in many moderate seismic regions. The seismic performance of these bridges is questionable. A portfolio of 30 non-seismically designed bridges is compiled for seismic reliability assessment. Fragility analysis is conducted, and the reliability of each structure is determined considering typical moderate seismic areas. The study shows that slab and multi-girder bridges with elastomeric bearings perform worse, whereas girder bridges with conventional bearings and multi-girder bridges with monolithic joints have better behavior. It is also shown that seismic design per Eurocode 8 leads to a reliability index of ~ 2 .

ARTICLE HISTORY

Received 4 July 2016
Accepted 5 February 2017

KEYWORDS

Seismic Performance of Highway Bridges; Multiple Stripes Analysis; Fragility Analysis; Seismic Risk Analysis; Moderate Seismicity; Seismic Reliability

1. Introduction

In moderate seismic areas, seismic risk mitigation efforts have lagged due to the fact that in these regions, large earthquakes are infrequent and may not have been experienced for over a century [Elnashai and Di Sarno, 2008]. The majority of the bridges were not designed for seismic loads due to the lack of proper seismic provisions in many countries of moderate and low seismic zones. For instance, as per the formal Hungarian road bridge standard ÚT [2004], only bridges with spans over 50 m had to be designed for seismic actions regardless of their other—often more relevant—parameters. Experience with existing and new structures [Zsarnóczy *et al.*, 2014; Simon *et al.*, 2015; Simon and Vigh, 2016] showed that a large portion of road bridges may be vulnerable to earthquake loads in moderate seismic regions. Since bridges are key elements of the infrastructure (their failure causes significant economic consequences: disruption to the traffic, transportation and emergency routes as well as economic loss and repair costs), it is an urgent and important issue to evaluate the seismic performance and vulnerability of conventional road bridges in these regions.

Comprehensive seismic performance evaluation of road bridges has been carried out in Central and Southeastern United States [Nielson, 2005; Padgett *et al.*, 2010], Italy [Borzi *et al.*, 2015; Zelaschi *et al.*, 2015a, 2016], Greece [Moschonas *et al.*, 2009], Turkey [Avşar *et al.*, 2011], and Algeria [Kibboua *et al.*, 2014]; however, most of these countries are characterized by high seismicity, where the bridges are possibly seismically designed leading to different structural characteristics and details in comparison to bridges in moderate seismic areas. Although Central and Southeastern United States is a moderate seismic region, there may be different design

CONTACT József Simon  simon.jozsef@epito.bme.hu  Department of Structural Engineering, Budapest University of Technology and Economics, Műegyetem rkp. 3-9, Kmf 85, H-1111 Budapest, Hungary.

Color versions of one or more of the figures in the article can be found online at www.tandfonline.com/ueqe.

traditions (e.g., Hungarian multi-span bridges are dominantly continuous, while simply supported versions are equally preferred in the Central and Southeastern United States) in other countries; besides, Nielson [2005] investigated only single-span and three-span overpass bridges on highways, while conventional large-span girder bridges are also typical structures in a bridge inventory.

In this study, a portfolio of 30 non-seismically designed road bridges is compiled based on the bridge inventory of Hungary. The bridges are selected to represent typical structures in moderate seismic zones. Multiple stripes analysis is adopted to create component and system fragility curves associated with three different damage limit states, using hazard-consistent recorded ground motions. Component fragility curves are used to determine critical bridge components, and system fragility curves are utilized to calculate the range of possible reliability levels considering representative moderate seismic regions, the highest and lowest seismic areas of Hungary.

2. Compilation of Representative Bridges

A portfolio of 30 representative, non-seismically designed bridges is compiled for seismic performance assessment in three steps: (1) with the statistical analysis of the Hungarian road bridge database [HTA, 2015], bridge types with the highest contribution to the highway bridge stock (either with value or number) are highlighted; (2) various classification approaches (e.g., [NIBS, 1999; Moschonas *et al.*, 2009; Avşar *et al.*, 2011]) are taken into account to select the eight representative bridge classes with possibly different seismic behaviors (Table 1); (3) as a result of multiple consultations with Hungarian bridge designer companies, specific realizations representing important and typical bridges are chosen for each bridge class. The selected bridges and their most important structural attributes are summarized in Table 2.

Figure 1a–d presents the most typical configurations, bridge components for the identified bridge classes. There are some general properties that are similar for all bridge types. The superstructure (SS) of multi-span bridges is mostly continuous; simply supported configurations are not common. The foundation system is pile foundation with very few exceptions. The main difference between the bridge classes is the superstructure-substructure joint type. PMG-I and SLAB bridges are constructed with monolithic joints (MJ1 and MJ2) both at the piers and abutments. PMG-NI bridges have monolithic joints (MJ2) usually at the middle piers; however, elastomeric bearings (EBs) are used at other piers and at the abutments, where expansion joints (EJs) are also applied to allow girder displacements in the longitudinal direction. Other bridges (RC-B, COMP-I, COMP-B, STEEL-I, STEEL-B) are usually constructed with conventional bearings free or fixed in one or two horizontal directions (generally

Table 1. Selected representative bridge types.

No.	Class type	Abbreviation	Bearing type	Typical bent type	Abutment type
1	Precast multi-girder	PMG-I	Monolithic	Multi-bent	Integral
2	Precast multi-girder	PMG-NI	Elastomeric + monolithic	Multi-bent	Seat type
3	RC slab	SLAB	Monolithic	Multi-bent	Integral
4	RC box girder	RC-B	Conventional bearing	Single bent	Seat type
5	Composite girder	COMP-I	Conventional bearing	Multi-bent	Seat type
6	Composite box girder	COMP-B	Conventional bearing	Multi-bent	Seat type
7	Steel girder	STEEL-I	Conventional bearing	Single bent	Seat type
8	Steel box girder	STEEL-B	Conventional bearing	Single bent	Seat type

Table 2. Structural attributes of the portfolio bridges (referred to with bridges number, e.g. BR25).

BR	Class	NS	Span lengths	TL	W	NFIX	NP	PCS	PH	ROS	FIW	SW	AW	SSW	JOINT
01	PMG-I	2	25-25	50	10	3	3	C	0.8	0.8	10	100	1571	18275	MJ1
02	PMG-I	2	25-25	50	18	3	5	C	0.8	0.8	10	100	1571	32700	MJ1
03	PMG-I	3	25-30-25	80	14	4	4	R	0.9	0.6	12	200	1131	32200	MJ1
04	PMG-I	3	18-30-18	66	14	4	3	R	0.9	0.6	16	150	2681	28950	MJ1
05	PMG-I	4	13-18-18-13	62	10	5	3	R	0.9	0.6	12	150	1508	17745	MJ1
06	PMG-I	4	15-17.5-17.5-15	65	15	5	4	R	0.9	0.6	12	150	1508	24635	MJ1
07	PMG-I	4	19-22-22-19	82	9	5	2	R	0.9	0.6	12	200	1131	14710	MJ1
08	PMG-I	6	11-15-17-17-15-11	86	12	7	3	C	0.8	0.8	10	100	1571	20232	MJ1
09	PMG-NI	3	35-45-35	115	14	2	4	C	1.2	1.2	12	200	1131	29795	MJ1+EB
10	PMG-NI	5	25-32-33-32-25	147	14	2	4	C	1.2	1.2	7	100	1047	29535	MJ1+EB
11	PMG-NI	6	30-4x45-30	240	14	3	3	C	1.2	1.2	12	100	2262	32155	MJ1+EB
12	PMG-NI	7	20-5x24-20	160	14	2	4	R	0.9	0.9	7	12	1131	28850	MJ1+EB
13	SLAB	2	25-25	50	9	3	2	R	0.9	0.6	12	150	1508	19650	MJ1+MJ2
14	SLAB	4	13-23-23-13	72	15	5	3	R	2.5	0.9	6	100	2356	34780	MJ1+MJ2
15	SLAB	4	12-22-22-12	68	12	5	2	R	0.9	0.6	12	200	1131	26200	MJ1+MJ2
16	SLAB	6	12-14-18-18-14-12	88	13	7	3	C	0.6	0.6	10	100	1571	29050	MJ1+MJ2
17	RC-B	5	5x34	170	11	1	1	R	6.0	2.0	14	200	4021	27800	CB
18	RC-B	6	37.5-4x50-37.5	275	14	1	1	R	4.9	2.0	15	200	4524	32500	CB
19	RC-B	7	36-5x45-36	297	17	1	1	R	6.0	2.8	24	12	3016	36485	CB
20	COMP-I	3	40-60-40	140	14	1	1	R	7.3	1.4	8	20	9425	21300	CB
21	COMP-I	3	75-90-75	240	14	1	1	R	12.0	3.3	7	16	22368	19700	CB
22	COMP-I	4	35-45-45-35	160	11	1	2	R	2.4	1.2	16	150	5362	18200	CB
23	COMP-B	3	24-36-24	84	14	4	4	R	1.1	0.6	16	100	4021	23700	MJ1+CB
24	COMP-B	3	35-45-35	115	14	1	2	C	1.6	1.6	5.5	1	2011	22000	CB
25	COMP-B	9	40-7x48-40	416	14	2	2	C	1.4	1.4	6.5	0.4	1131	22000	CB
26	STEEL-I	5	5x50	250	14	1	2	R	2.0	1.2	5.5	1.25	150	15500	CB
27	STEEL-I	9	23-3x45-60-3x45-23	375	14	2	2	R	2.0	1.2	5.5	1.25	150	15500	CB
28	STEEL-B	2	80-80	160	15	1	2	R	1.5	1.5	1.3	16	150	16500	CB
29	STEEL-B	3	3x110	330	22	1	1	R	13.0	3.5	16.5	16	250	17500	CB
30	STEEL-B	8	60-6x80-60	600	14	1	2	R	1.5	1.5	1.3	16	150	8043	CB

NS – number of spans; TL – total length [m]; W – width [m]; NFIX – number of fixed bearings in the longitudinal direction; PCS – pier cross section size [m] (C: circular; R: rectangular); PH – pier height [m]; ROS – pier longitudinal reinforcement ratio [%]; FIW, SW, and AW – pier shear reinforcement diameter and distance [mm], total area [mm²]; SSW – superstructure mass [kg/m]; JOINT – joint type: MJ1 and MJ2 – monolithic joint Type 1 and 2; EB – elastomeric bearing; CB – conventional bearing.

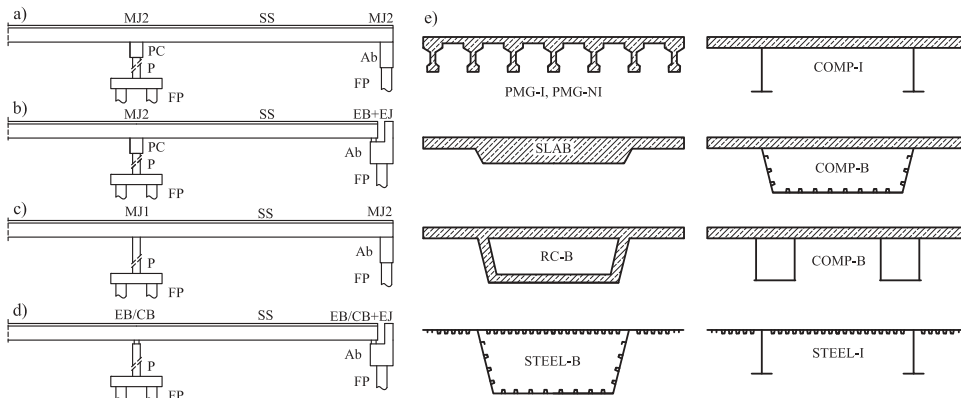


Figure 1. Typical bridge configurations: (a) PMG-I, (b) PMG-NI, (c) SLAB, (d) other conventional girders, and (e) cross sections of each bridge class. For component codes, see Fig. 2.

on one or just some of the piers in the longitudinal, while on all the piers in the transverse direction). Pier cap (PC) beams are used for PMG-I and PMG-NI bridges to provide proper support for the precast beams, while piers are joined directly to the deck in case of SLAB bridges. The abutment is integral type with monolithic joints (MJ2) for PMG-I and SLAB bridges, and seat type for other bridge classes with the application of elastomeric (EB) or conventional bearings (CBs) and EJ.

3. Numerical Modeling

3.1. General Description

A 3-dimensional beam element model is implemented in OpenSees [McKenna *et al.*, 2010] (Fig. 2a). The main structural elements (piers, superstructure, abutments, etc.) are modeled with two-node beam elements with 6 degrees of freedom per node, while nonlinear springs are used to model the flexible supports, the soil-structure interaction, and the bearings. The beam elements are placed in the center of mass, while eccentricity between the member axes is bridged over with rigid elements. The mass of the structure and the additional dead load are lumped into nodes.

3.2. Superstructure and Pier Cap Beam

Plastic deformation of the superstructure and the PC beam is not expected as it is concluded for typical girder bridges by Zsarnóczy *et al.* [2014]; therefore, linear elastic behavior is assigned to these components (*elasticBeamColumn* element).

3.3. Superstructure-Substructure Joints

In case of CBs, spring elements are placed at each bearing position (Fig. 2b, detail B), while continuous monolithic joints are approximated with discrete contact points (Fig. 2b, detail A). The constitutive models for bearings and EJs are presented in the following subsections.

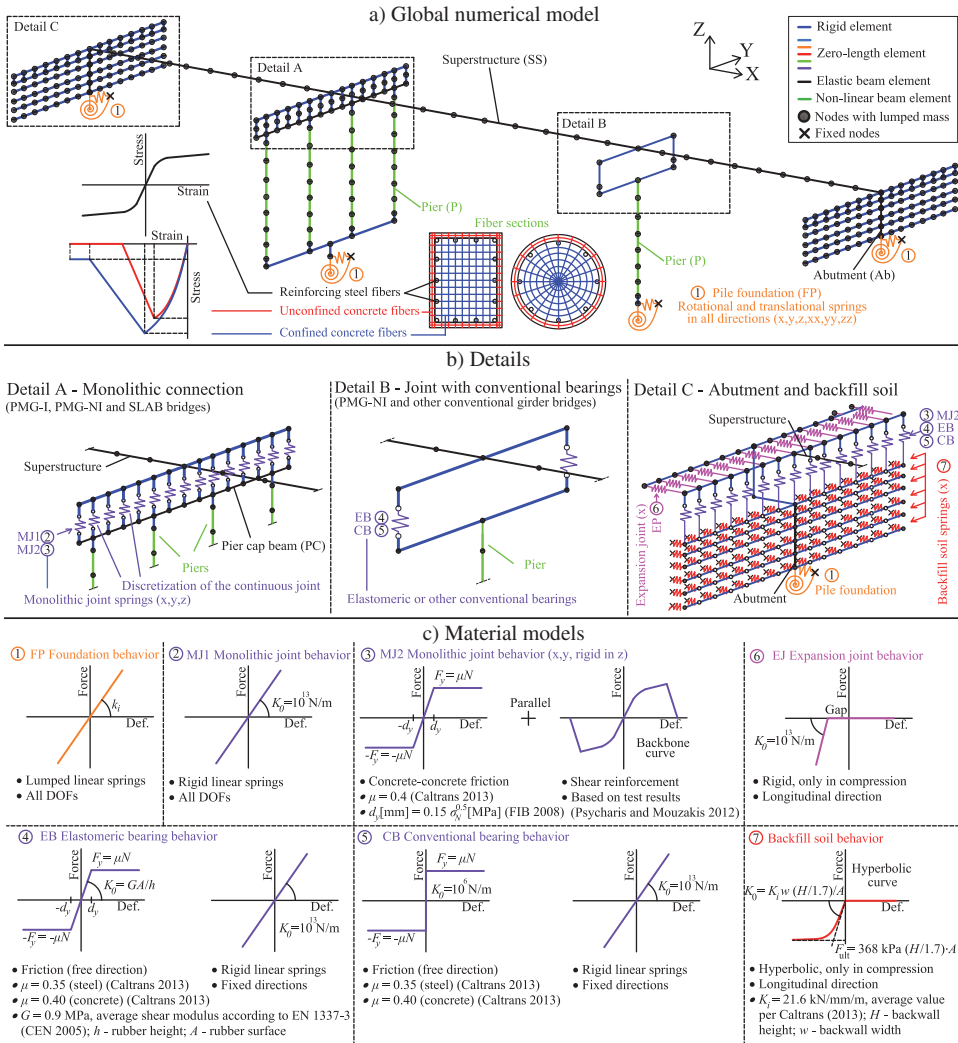


Figure 2. Numerical model. (a) Global numerical model, (b) details, and (c) material models.

3.3.1. Monolithic Joints

There are two typical monolithic joints (Fig. 3): (1) piers are joined directly to the deck in case of SLAB bridges (MJ1); and (2) vertical reinforcement is applied to transfer lateral forces for PMG bridges (MJ2). MJ2 is commonly used for SLAB bridge abutment joints as well. MJ1 joints can be characterized with complex behavior transferring both shear forces and bending moments. Design and verification of such joints are based on the limitation of maximum shear stress in the middle point. MJ1 monolithic bridge joints were studied with laboratory tests by many researchers (detailed literature can be found in [Timosidis *et al.*, 2015]); however, there are only a few suggestions for the modeling. Although Timosidis and Pantazopoulou [2009] proposed a uniaxial backbone curve for the shear stress-shear deformation relationship, the input parameters hold a lot of uncertainties. Moreover, degradation and other cyclic parameters are needed for proper modeling. In typical bridge configurations,

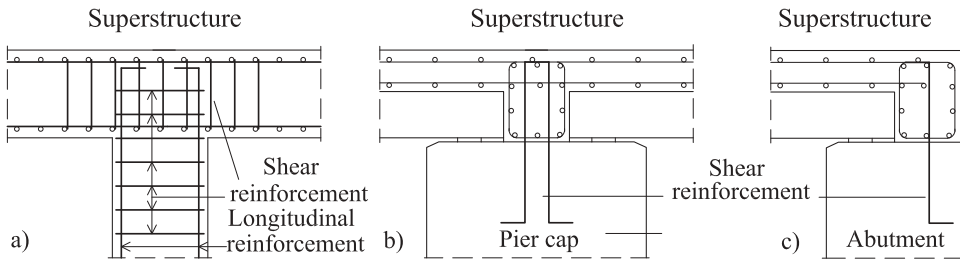


Figure 3. Typical monolithic joints. (a) Piers are joined directly to the deck (MJ1). Shear reinforcement is applied between: (b) the deck and the pier cap (MJ2); (c) the deck and the abutment (MJ2).

MJ1 joints show significantly higher resistance compared to the pier. For instance, if a typical RC slab bridge is considered, the shear forces associated with cracking of the joint is two times larger than the pier shear resistance. For this reason, and also due to the uncertainties in the input parameters and modeling, MJ1 monolithic joints are incorporated as rigid connections both for displacements and rotations (Fig. 2c, material model 2).

The behavior of MJ2 joints is simpler. Because only shear reinforcement is applied, they can be characterized with semi-rigid flexural behavior. The rotational stiffness of the joint is negligible compared to the bending stiffness of the adjacent structural elements (e.g. pier, superstructure); therefore it can be best approximated as hinged [Fennema *et al.*, 2005]. During the rotation of the joint, cracks may appear, and hence reliable estimation of the concrete shear strength cannot be given. Therefore, MJ2 joints are modeled with two material models working parallel to take into account the cyclic behavior of the vertical rebars and the friction between the two concrete surfaces (Fig. 2c, material model 3). The latter is modeled using a bilinear model (*Steel01* material), while material model calibration (*Pinching4* material) [Simon and Vigh, 2016] is carried out to model the cyclic behavior of the shear reinforcement based on laboratory test results of pinned connections with $2\phi 16$ vertical rebars [Psycharis and Mouzakis, 2012].

3.3.2. Conventional Bearings

The most commonly used bearing type is the elastomeric bearing. The behavior in the free horizontal direction can be characterized by a bilinear curve (Fig. 2c, material model 4). The stiffness of the elastomeric bearing is associated with the shear stiffness of the rubber bearing, while the shear capacity is calculated as the dynamic friction capacity considering a friction coefficient of 0.4 for concrete and 0.35 for steel surfaces [Caltrans, 2013]. In the fixed direction, the behavior is highly dependent on the actual configuration and restrainer components. Ultimate resistance of the bearings could be estimated from the design forces of the ultimate limit state; however, cyclic and even post-yielding behaviors are unpredictable without laboratory tests or detailed finite-element models. For this reason, a simplified modeling is followed: bearing stiffness is fully rigid in the restrained direction, while their failure is not incorporated in the model (infinite strength is assumed) (see Fig. 2c, material model 5). The same assumption applies for other CBs in this study. Note that the decreased stiffness due to yielding leads to lower seismic demands of the piers, abutments, and foundations; thus, it is a conservative approach with regard to these important components maintaining the structural integrity of the structure.

3.3.3. Expansion Joint

The gap in the expansion joint can be modeled directly with separate components and contact elements to recognize pounding. However, it is a difficult task to set proper parameters for the contact stiffness to avoid convergence problems and excessive calculation time. A simpler approach is followed: the gap is integrated in the constitutive model with high stiffness (to model rigid contact) and infinite strength (*ElasticPPGap* material) (Fig. 2c, material model 6).

3.4. Piers

Piers are modeled with nonlinear beam elements (*dispBeamColumn* element), material nonlinearity is taken into account with fiber sections (see Fig. 2a), while geometric nonlinearity (P- Δ effect) is also incorporated. Uniaxial constitutive models assigned to the fibers are the Scott-Kent-Park concrete model (*Concrete01* material) and the Giuffr -Menegotto-Pinto reinforcing steel model (*Steel02* material). Confined concrete properties are calculated per EC8-2 [CEN, 2008b] Annex E. Note that due to the low shear reinforcement ratio (<0.75%), the increase of strength and ductility of the confined concrete is usually not significant (<10%).

3.5. Abutments and Backfill Soil

The abutment can be regarded as a rigid block, and stability failure is more possible than failure due to inadequate strength. Therefore, abutments are modeled with simple linear elastic behavior (*elasticBeamColumn* element). As part of the Caltrans seismic research program, full-scale abutment field experiments were conducted [Maroney, 1995]. The test results showed hyperbolic force-deformation behavior of the abutment-backfill soil system subjected to monotonic longitudinal loading [Shamsabadi *et al.*, 2007]. This hyperbolic behavior is implemented in the model through compression-only nonlinear spring elements (*ZeroLength* element) with adjusted spring characteristics (*HyperbolicGap* material) and plastic behavior (Fig. 2c, material model 7). One end of the springs is attached to the nodes of a rigid grid modeling the surface of the abutment; the other end is attached to fixed nodes (Fig. 2b, detail C). The initial stiffness of the hyperbolic curve is calculated per Caltrans [2013] from an initial stiffness value (K_i) determined for the entire width (w) of the bridge. The stiffness is adjusted to the backwall height (H) lumped into the nodes proportionally to the corresponding areas (A). The ultimate force (F_{ult}) is lumped into the surface nodes in the same way, where 368 kPa maximum passive soil pressure is utilized for dynamic loads per Caltrans [2013]. In Simon and Vigh [2016], it was concluded that the participating mass of the backfill soil, the approaching slab, and the wing walls have insignificant influence in case of longer bridges (>50 m). Since all the examined bridges are longer than 50 m, the above-mentioned components are not incorporated in the numerical model for simplification.

3.6. Foundation

The dynamic impedance of the soil-foundation system can be approximated through assemblies of springs, dashpots, and fictitious masses [Wolf, 1985]. The complex impedance is frequency dependent, where the complex part represents radiation damping in the soil. As a conservative

approach, both radiation and material damping of the soil are neglected in this study, and linear springs are used (*ZeroLength* element) to take into consideration the translational and flexural stiffness of the pile foundation (Fig. 2c, material model 1). The vertical stiffness of an individual pile is determined as the initial stiffness of a simplified trilinear behavior, representing the combined behavior of skin friction and tip resistance; and the estimation of the horizontal stiffness is given according to EC8-5 [CEN, 2009] Annex C. The translational and rotational stiffness of the foundations is calculated directly from the vertical and horizontal stiffness of the piles accounting for the actual layout of the foundation system.

4. Reliability Assessment

4.1. Adopted Method for Fragility Analysis

State-of-the-art seismic vulnerability assessment is based on analytical fragility curves [Billah and Alam, 2015] created with nonlinear time-history analysis (NLTHA). Fragility curves are conditional probability statements giving the probability of reaching a particular limit state (LS) for a given intensity measure (IM) level. For the unconditional probability of failure, the IM exceedance rate for the reference period is needed, which is provided by the seismic hazard curve of the site. Note that failure does not necessary mean collapse, it only shows that the structure reached a predefined LS. Fragility analysis is a useful tool, since it enables retrofit decisions regarding economical and financial aspects.

Widely applied methods exist for fragility analysis such as Incremental Dynamic Analysis (IDA) [Vamvatsikos and Cornell, 2002] and Multiple Stripes Analysis (MSA) [Jalayer and Cornell, 2009]. The study adopts MSA for two reasons: (1) it is proved to be more efficient fragility estimates than IDA for a given number of structural analyses [Baker, 2015]; (2) it allows for different ground motions to be used at varying intensity levels to represent the differing characteristics of low- and high-intensity shaking. The steps of the MSA procedure are presented in Fig. 4a. At each intensity level, a number of ground motions are selected for each horizontal direction. Maximum demands are registered during NLTHA, then assuming lognormal (LN) distribution, the median and the coefficient of variation (CoV) are calculated for the demands. A single fragility point at an intensity level is obtained as follows:

$$P[(D > C_{LSi})|IM] = \int_0^{\infty} P(D > \alpha | IM) P(C_{LSi} = \alpha) d\alpha, \quad (1)$$

where D is the calculated seismic demand; C_{LSi} is the capacity associated with the i th LS; the second function is the probability density function of the capacity, and α denotes integration over the demand parameter. The probability of component failure can be computed as:

$$p_i = \int_{IM} P[(D > C_{LSi})|IM] d\lambda(IM), \quad (2)$$

where $d\lambda$ is the derivative of the hazard curve (Fig. 4b).

In this study, the reliability index β calculated with the inverse standard normal cumulative density function (CDF) is used to compare the seismic performance of different bridge configurations:

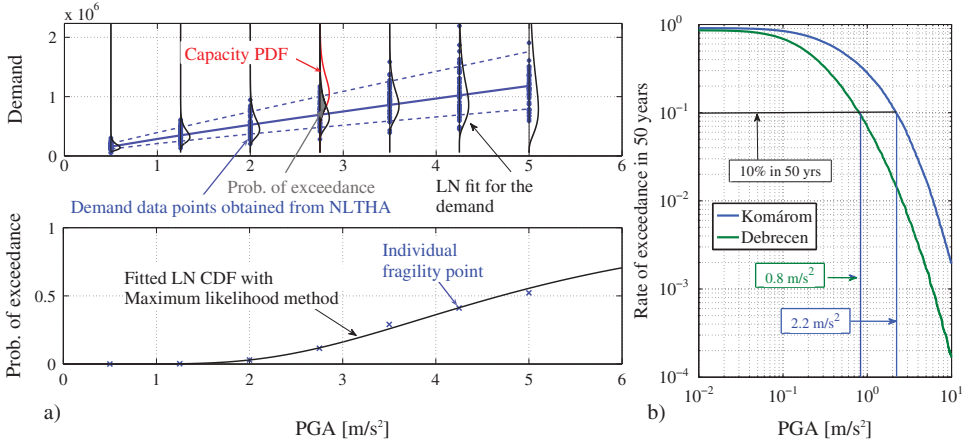


Figure 4. (a) Procedure of the Multiple Stripes Analysis and (b) PGA hazard curve for Komárom and Debrecen considering soil type C.

$$\beta_i = -\Phi^{-1}(p_i). \quad (3)$$

The component fragility curves are useful to highlight critical components, and to calculate the probability of component failure; however, a system fragility curve is required to determine the probability related to the whole structure. It is assumed that bridges compose series systems (system failure is associated with the failure of any component). Using first-order reliability theory, a simple lower and upper bound on the system fragility (P_{sys}) can be determined for an m component system with P_i component probabilities at a given IM level:

$$\max_{i=1:m} P_i \leq P_{sys} \leq 1 - \prod_{i=1}^m [1 - P_i]. \quad (4)$$

The lower bound represents a system where the components are fully stochastically dependent (unconservative estimate), while the upper bound assumes that the components are all statistically independent (conservative estimate) [Nowak and Collins, 2000]. Additionally, Monte-Carlo (MC)-type simulation is applied to give a better estimation based on the joint distribution of the demands and capacities assumed to be multivariate LN (MLN) distributions [Nielson, 2005]. At each IM level, the marginal distribution of the component demands is obtained during the MSA procedure, and then the cross-correlation is computed to fully describe the distribution of the demands. The capacities are also estimated with an MLN distribution, but in this case, the correlation between each component capacity is not known. Accordingly, two cases are examined: full correlation or no correlation at all (regarding the capacities). The idea of the simulation is to generate a large number of random samples from the demand and capacity MLN distributions, then P_{sys} is determined by taking into account the ratio of the cases of failure and the number of simulated cases. This can be done for various IM levels to compose the individual points of the system fragility curve.

In this study, peak ground acceleration (PGA) is selected as the main IM for three reasons: (1) as noted by Bradley [2012a], the probability of failure is independent of the chosen IM if hazard-consistent ground motions are selected (Sec. 4.2); (2) comparison between fragility curves is easier with a general IM such as PGA; (3) PGA is widely applied by researchers for the fragility

evaluation of bridges [Nielson, 2005; Zelaschi *et al.*, 2015b]. Ten ($0.5:0.5:5 \text{ m/s}^2$) intensity levels are chosen, and 50 tri-directional ground motions (two horizontal and one vertical component) are selected for each level in all cases considering soil type C ($v_{s30} < 360 \text{ m/s}$) per EC8-1 [CEN, 2008a]. One could model the different site amplification and filtering by the foundation as well as the effect of wave propagation by using different prescribed ground motions as input at various supports of the structure, see for example [Sextos *et al.*, 2003a, b; Pinto and Franchin, 2010]. However, due to the difficulty in predicting the values of the parameters of current models for the simulation of differential input, spatial variability of the seismic action is not taken into account. Note that according to EC8-2, this issue should be investigated only for 5 of the 30 examined bridges.

4.2. Ground Motion Selection

A state-of-the-art General Conditional Intensity Measure (GCIM) ground motion (GM) selection procedure [Bradley, 2010, 2012b] is adopted in this study. The idea is similar to that presented in [Baker, 2011], deriving the distribution of a vector of IMs conditional on the main IM from their joint MLN distribution. The novelty of the GCIM method is that the IM vector can consist of not only spectral accelerations (Sa) but also other IMs (such as energy content or duration measures). The conditional distribution provides the theoretical distribution of potential GMs, which may be observed at the site; therefore, GM selection can be carried out fully consistently with the seismic hazard. Bradley [2012b] proposed a selection procedure similar to that of Jayaram *et al.* [2011]: a number of random realizations are generated from the theoretical distribution, and then GMs with the smallest residual for each realization are selected. Additionally, Bradley [2012b] suggested that multiple realization sets should be generated, and finally the ground motion pack with the smallest Kolmogorov-Smirnov test statistic (which defines the difference between the target distribution and the empirical distribution of the GM set) should be selected.

The record selection is carried out for the area of Komárom and Debrecen selecting three-component GMs, considering soil type C, and using the strong motion database of the Pacific Earthquake Engineering Research Center [PEER, 2015]. The selection is based on the geometric mean of the IMs of the horizontal directions; however the vertical components of the selected records are also applied to the structure during the analysis. The bridge inventory is diverse; therefore, it is most advantageous to select a vector of IMs that measure different properties of the GM and correlate well with the seismic response of a wide range of different bridge configurations. PGA and spectral acceleration (Sa) at $T_0 = \{0.1:0.1:0.8, 1.0, 2.0, 3.0, 4.0\}$ s are considered to account for GM intensity over a wide range of vibration periods; and additionally, acceleration spectrum intensity (ASI), peak ground velocity (PGV) as well as velocity spectrum intensity (VSI), and displacement spectrum intensity (DSI) are included for acceleration, velocity, and displacement sensitive structures, respectively. These parameters represent peak responses; however, to describe cumulative phenomena, absolute velocity (CAV)—which accounts for the amplitude, frequency content and duration of GM in a cumulative manner [Campbell and Bozorgnia, 2010]—and significant duration (D_{s575} and D_{s595})—which approximately indicate durations of body and surface waves [Bommer and Martinez-Pereira, 1999]—are also incorporated. Therefore, the IM vector consists of the following 20 elements: {PGA, Sa($T_0 = [0.1:0.1:0.8, 1.0, 2.0, 3.0, 4.0]$ s), PGV, ASI, VSI, DSI, CAV, D_{s575} , D_{s595} }. According to Bradley [2012b], the importance of different IMs should be

taken into account by assigning different weights to them. The weights are set equally, thus the total weight of the most important IMs related to peak responses is 0.85, while a total weight of 0.15 is assigned to the other IMs associated with cumulative behavior. PGA hazard is calculated using the ground motion prediction model (GMPM) of Akkar and Bommer [2010]; references to other GMPMs and the equations to calculate the correlation structure for the joint distribution can be found in Bradley [2012b].

An example record selection is presented for Komárom: the theoretical distributions (conditioned on the design PGA level: 10% probability of exceedance in 50 years) of some selected IMs and the empirical CDF of the selected 50 GMs are shown in Figs. 5a, and Fig. 5b presents the spectra of the selected records. The theoretical distributions are useful to analyze the expected earthquake characteristics. For instance, the median significant duration is only ~ 7 s. According to EC8, when site-specific data are not available, the minimum duration of the stationary part of the accelerograms should be equal to 10 s. Considering the expected characteristics of possible earthquakes may lead to a decreased duration of the seismic load and less conservative seismic demands, especially in the case of structures with rapid rates of cyclic deterioration and accumulating plastic deformations [Chandramohan *et al.*, 2015].

4.3. Damage Limit States

Three damage LSs per Priestley *et al.* [1996] are considered that can be associated with the Damage Limitation (LS1), Significant Damage (LS2), and Near Collapse (LS3) LSs of EC8-3 [CEN, 2011a] (Table 3). The capacities of the bridge components are assumed to follow a LN distribution per EC0 [CEN, 2011b]. In case of shear failure, CoV value is assigned according to Biskinis *et al.* [2004]. The other LSs are determined in a prescriptive manner (the thresholds are defined by the analyst) with assigned CoV values of 0.25, 0.30, and 0.35 [Nielson, 2005].

4.4. Uncertainties Applied During the Analysis

MSA can be regarded as a simplified MC simulation, where the capacity distribution is known and the distributions of the demands are determined independently from a

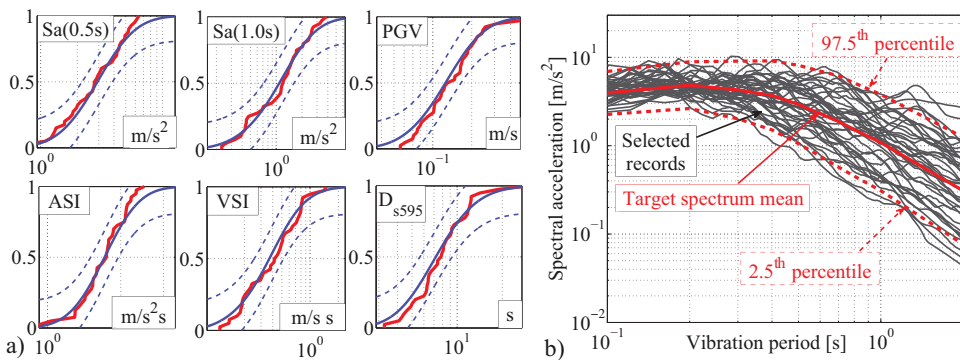


Figure 5. (a) Theoretical distribution of some IM conditioned on PGA (solid blue line). Blue dashed line: KS bounds (0.1 confidence level); solid red line: empirical distribution of the selected records and (b) acceleration response spectra of the selected records.



Table 3. Limit states and associated capacities. Detailed information on the limit state median values can be found in Appendix A.

Component	Measure	Definition			Median			CoV		
		LS1	LS2	LS3	LS1	LS2	LS3	LS1	LS2	LS3
Pier flexural	Steel or concrete strain	Yielding of rebars	Spalling of concrete	Crushing of concrete	0.28%	0.3% ¹	VA ²	0.25	0.30	0.35
Pier shear ³	Shear force	Shear failure	Shear failure	Shear failure	VA ⁴	VA	VA	0.25	0.25	0.25
Type 2 monolithic joint ⁵	Deformation	Yielding	Strength degradation	Unseating ⁶	2 mm	50 mm	VA	0.25	0.30	0.35
Elastomeric bearing ⁷	Deformation	Yielding	Girder falls off from pedestal	Unseating	70 mm ⁸	VA ⁹	VA	0.25	0.30	0.35
Conventional bearing ¹⁰ – free ¹¹	Deformation	Girder falls off from pedestal	Girder falls off from pedestal	Unseating	VA	VA	VA	0.25	0.30	0.35
Backfill soil ¹²	Deformation	Yielding	Minor damage	Abutment instability	30 mm	60 mm	300 mm	0.25	0.30	0.35

VA – various values for different configurations.

1 - Priestley et al. [1996].

2 - Determined with moment-curvature analysis of the pier cross-section.

3 - Brittle failure mode. Only one limit state is defined.

4 - Calculated according to Priestley et al. [1996] considering the contributions from concrete resistance, axial force and transverse steel.

5 - Used for PMG-I, PMG-NI and SLAB bridges with the presented capacities based on the cyclic behavior.

6 - Depends on the dimensions of the support. Measured as the closest distance from the supporting axis to the edge of the support.

7 - Used for PMG-NI bridges.

8 - Calculated from typical bearing properties applied for PMG-NI bridges.

9 - Depends on the dimensions of the support. Measured as the closest distance from the supporting axis to the edge of the pedestal.

10 - Used for RC-B, COMP-I, COMP-B, STEEL-I and STEEL-B bridges to model unrestrained horizontal behavior.

11 - Due to the uncertainty of the actual capacities, this component is not evaluated in the fixed direction.

12 - Capacity values are in accordance with EC8-2 (yielding, damage control limit, excessive deformation).

reasonably large number of time-history analyses at each intensity level. The uncertainty of the demands is controlled mainly by the seismic load. However, to take into account other uncertainties in the phase of determining the demands, material properties and other input parameters are considered as random variables (Table 4). For each time-history analysis, a random sample is used to create the numerical model of the bridge. This approach is not only straightforward but also computationally demanding. It should be noted that the efficiency could be increased using the Latin Hypercube sampling method, as shown by Monteiro *et al.* [2016a, 2016b] and Monteiro [2016].

4.5. Effect of Various Modeling and Analysis Assumptions

Two modeling issues are investigated before the fragility analysis: (1) monolithic joints and; (2) EJs. Figure 6 shows the NLTHA results for a PMG-I example bridge with or without modeling the nonlinear behavior of the monolithic joints. Figure 6b indicates that due to the high seismic demands, strength degradation of the shear reinforcement occurs and eventually the resistance is reduced, and only frictional forces develop. This degradation leads to the redistribution of seismic demands: pier demands (Fig. 6a) and shear forces in the pier joint (Fig. 6c) may be significantly increased compared to the model where the joint is modeled as a rigid connection.

In case of bridges with EJs, the pounding between the abutment and the superstructure may significantly alter the seismic response. The phenomenon is illustrated in Fig. 7 for a composite bridge with a 65 mm expansion joint gap. The pounding may decrease the demands of the piers: excessive displacements, thus the second-order effects are reduced, while a portion of the seismic force is transferred to the abutment-backfill soil system (Fig. 7a). Figure. 7b shows that the pounding limits the expansion joint compressive

Table 4. Random variables applied to sample input for the numerical model.

Variable	Distribution	Mean/median	STD/COV	Reference
Pier cross section	Uniform ¹	VA	± 20 mm	-
Pier height	Uniform	VA	± 50 mm	-
Superstructure mass	Normal	VA	0.1	Nowak and Collins [2000]
Reinforcement ratio	Uniform	1%	± 0.3%	-
Expansion joint gap	Uniform	VA	± 65% ²	-
Concrete compressive strength	Lognormal	38 MPa ³	0.15	JCSS [2001]
Reinforcing steel yielding	Normal	598 MPa ⁴	0.1	JCSS [2001]
Friction coefficient (concrete-concrete) ⁵	Uniform	0.4	± 0.1	-
Elastomeric bearing shear modulus	Uniform	0.9 MPa ⁶	± 50%	Nielson [2005]
Elastomeric bearing friction coefficient	Lognormal	VA ⁷	0.1	Dutta [1999]
Foundation stiffness	Uniform	VA	± 50%	Nielson [2005]
Backfill soil stiffness	Uniform	21.6 kN/mm/m	± 7.2 kN/mm/m ⁸	Nielson [2005]
Earthquake direction	Uniform	π/4 rad	± π/4 rad	Nielson [2005]

VA – various values.

1 - When sufficient information on probability distributions is not available, it is acceptable to assume a uniform distribution with reasonable upper and lower limits to roughly account for uncertainty [Nielson, 2005].

2 - Assumption: the expected thermal movements are between ± 65% of the designed gap value.

3 - Bridges are built with C30/37 concrete grade.

4 - S500 steel grade is assumed for all the bridges.

5 - Used in case of Type 2 monolithic joints.

6 - Average shear modulus according to EN 1337-3 [CEN, 2005].

7 - 0.35 and 0.4 for steel and concrete superstructure, respectively [Caltrans, 2013].

8 - Based on the upper and lower value of 14.4 and 28.8 kN/mm/m proposed by Caltrans [2013].

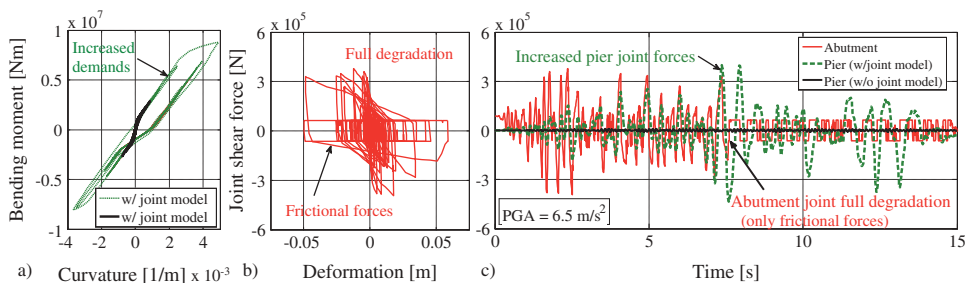


Figure 6. NLTHA results with or without modeling the Type 2 joint behavior for a PMG-I example bridge (BR03). (a) Pier moment-curvature diagram, (b) abutment joint behavior and (c) abutment and pier joint shear forces.

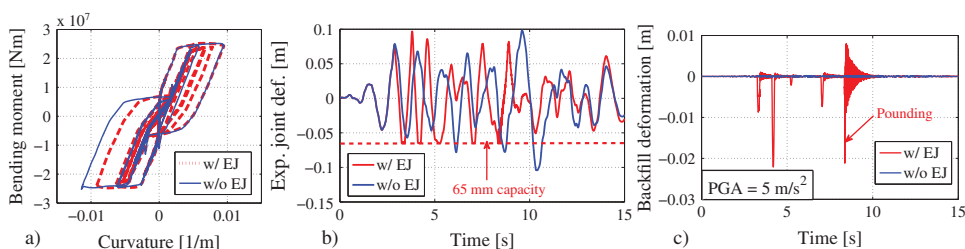


Figure 7. NLTHA results with or without modeling the expansion joint (EJ) behavior for a COMP-I example bridge (BR20). (a) Pier moment-curvature diagram, (b) expansion joint deformation and (c) backfill soil deformation.

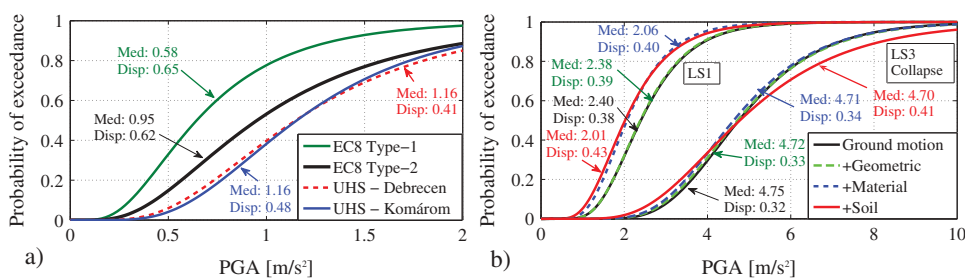


Figure 8. Comparison of fragility curves: (a) using different spectra and sites for the BR24 bridge (pier shear failure) and (b) taking into account GM direction, geometric, material, and soil uncertainties for the BR01 bridge (system fragility curves).

deformations, while in Fig. 7c, a pulse-like peak can be observed in the backfill soil deformation when collision occurs.

As a second step, fragility curves are created considering different analysis assumptions: (1) using different spectra; (2) considering different sites; and (3) considering uncertainties in the input parameters. The derived fragility curves are highly dependent on the spectral shape (Fig. 8a). Artificial records are generated for two standard spectra (EC8 Type 1 and 2), and GCIM selection is carried out for two sites (Komárom and Debrecen). The application of

artificial records is convenient to consider standard specified design loads, since they can be matched exactly to the standard spectrum. However, to incorporate record-to-record variability, the amplitudes of the artificial records are multiplied with a random factor considering a lognormal distribution of 1.0 median and 0.5 standard deviation [Jernigan and Hwang, 2002]. As confirmed by Fig. 8a, the Type 2 standard spectrum represents moderate seismic areas better than the Type 1 spectrum. The fragility curve derived with the Type 2 spectrum is closer to the site-specific ones. It can also be observed that there is only a slight difference between fragility curves created for different sites. It implies that the general seismic characteristics are just slightly different; therefore, it might be sufficient to derive fragility curves for only one site and use it for other areas in Hungary without introducing significant error in the results.

The uncertainty of the fragility results stems mainly from the uncertainty of the seismic load itself. A short parametric study is conducted—similar to the one carried out by Padgett and DesRoches [2007]—to understand the effect of other sources of uncertainty (Fig. 8b). In Table 4, random variables applied to sample input for the numerical model are presented. Fragility curves are created for LS1 and LS3 for an integral PMG-I bridge considering first only GM direction uncertainty, then additionally geometric, material, and soil uncertainties are also applied. It is shown that the geometric uncertainty has negligible effect, while the material and soil uncertainties may significantly influence the calculated probability of failure. The material uncertainty is dominant when the LS is associated with yielding and plastic deformations (e.g., LS1 in Fig. 8b is controlled by the yielding of the abutment joint); while in case of LS with dominant brittle failure mode (e.g. LS3 in Fig. 8b is controlled by the pier shear failure), soil uncertainties significantly influence the dispersion of the demands.

In conclusion, the fragility evaluation is conducted: (1) with a robust and detailed numerical model; (2) using the site-specific spectrum for Komárom considering soil type C; (3) applying 50 tri-directional selected GMs at 10 intensity levels; (4) incorporating the uncertainties listed in Table 4.

5. Results

5.1. Fragility Curves

5.1.1. Precast Multi-Girder (PMG-I) Bridges with Monolithic Joints

BR01-BR08 are PMG-I bridges where all joints are MJ2 monolithic joint (see Fig. 3). Their typical damage mechanism is illustrated through the results of the BR07 configuration (Fig. 9). It is highly possible that the abutment joint yields in the longitudinal direction and even transverse yielding of the abutment joint is expected to occur prior to the pier damage. The probability of backfill soil damage is nearly zero in the observed range of PGA. It can be

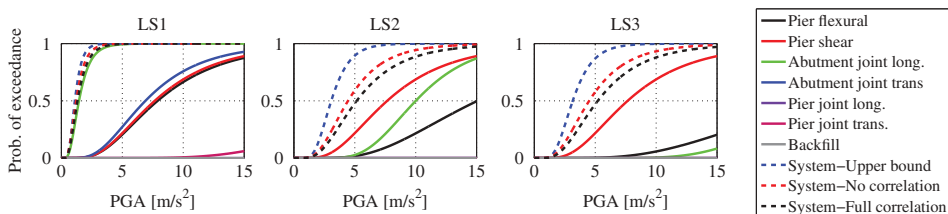


Figure 9. Fragility curves for the BR07 (PMG-I) bridge.

concluded that the fragility of the system in LS1 is driven by the abutment joints. It is considered that after the joints yield, the bridge is still functional; LS2 is associated with the ultimate deformation capacity and full degradation of the joint rebars. The probability that the joints reach LS2 is lower. Since PMG-I bridges usually have relatively short piers (5–6 m), there is a high probability that pier shear failure occurs before other components reach LS2, meaning that the bridge collapses with an unfavorable brittle failure mode right after the yielding of the system.

If the pier height is increased, shear failure becomes less dominant. BR04 is an example for this (Fig. 10), as it has relatively high piers (9 m) leading to low shear forces; besides, the shear reinforcement is high ($\phi 16/150$) compared to the other configurations. Similar to other PMG-I bridges, the abutment joint resistance is inadequate, and this component controls LS1 and LS2. However, in LS3, the bridge is more likely to suffer flexural failure, and due to the high shear resistance, a ductile behavior can be achieved. The unseating of the superstructure (associated with joint deformations in LS3) is possible, but the probability is far lower than the probability of flexural failure.

In Fig. 11, system fragility curves are illustrated. LS1 fragility curves show the same tendency, except for BR03 where the abutment joint is more likely to yield. This is the only configuration with low ($\phi 16/200$ instead of $\phi 16/150$) shear reinforcement of this joint. For most bridges, LS2 and LS3 are nearly identical since shear failure dominates before other components reach LS2 or LS3.

5.1.2. Precast Multi-Girder (PMG-NI) Bridges with Elastomeric Bearings

The other type of precast multi-girder bridge (PMG-NI; BR09–12) is constructed with EBs at some piers to provide free movements in case of longer bridges; and monolithic joint with shear reinforcement (MJ2) is applied at certain piers to provide restraint in the two horizontal directions. These bridges are more flexible with increased fundamental periods in both directions. For this reason, one would expect lower seismic demands; however, the lower

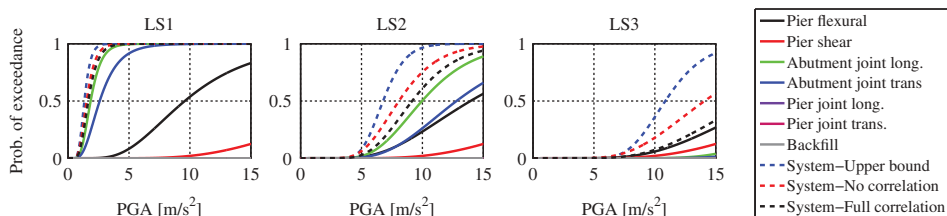


Figure 10. Fragility curves for the BR04 (PMG-I) bridge.

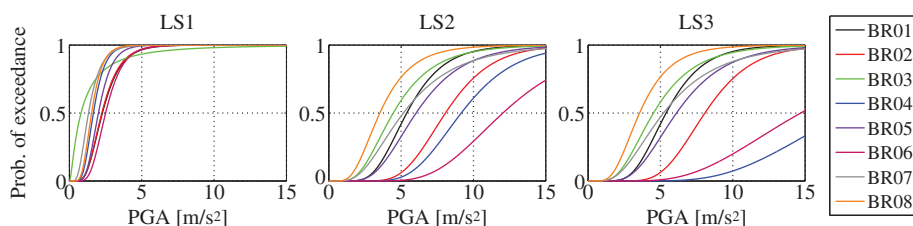


Figure 11. System fragility curves (full correlation in capacity) for PMG-I bridges.

base shear force is distributed on fewer piers. The high vulnerability of PMG-NI bridges is illustrated in Fig. 12 showing that pier shear failure develops prior to any other component damage. This is confirmed by the system fragility curves (Fig. 13), and no significant difference in the system fragilities of different LSs can be observed.

The component fragility curves provide some additional information about the bridge performance. Besides the piers, there are other components that may be vulnerable because of the structural layout. Typically, monolithic joints are created in the middle piers, while on the abutments, EBs and EJs are constructed. If pounding occurs, it increases the probability that the backfill soil reaches a given damage LS. There is also higher probability of unseating because of the excessive movements compared to integrate PMG-I bridges. Figure 12 shows that the backfill failure and unseating would be more likely than pier flexural failure in LS3, if the pier shear resistance was sufficient.

5.1.3. Reinforced Concrete Slab (SLAB) Bridges

SLAB bridges may be characterized by the same behavior as PMG-I bridges, except that higher demands are calculated due to the integrated monolithic joint MJ1. Similar behavior is confirmed by the component fragility curves in Fig. 14: LS1 is associated with abutment

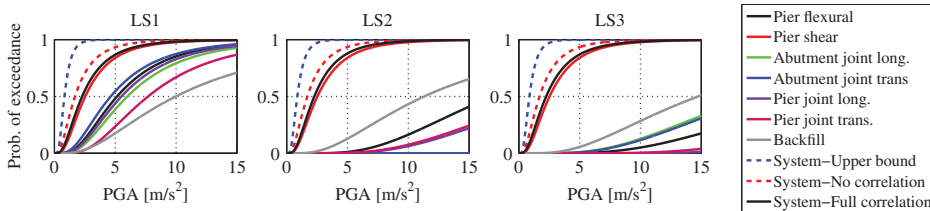


Figure 12. Fragility curves for the BR10 (PMG-NI) bridge.

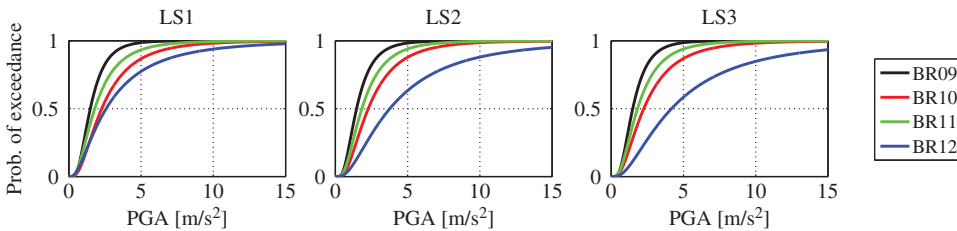


Figure 13. System fragility curves (full correlation in capacity) for PMG-NI bridges.

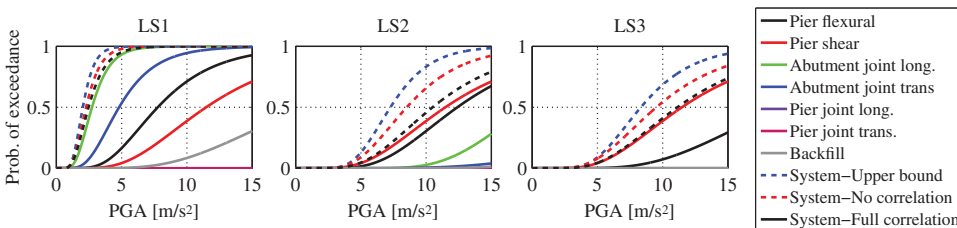


Figure 14. Fragility curves for the BR13 (SLAB) bridge.

joint yielding, while pier shear failure is dominant in LS3 (and also in LS2) for the examined slab bridges as well (see also system fragility curves in Fig. 15).

5.1.4. Reinforced Concrete Box-Girder (RC-B) Bridges

Results for RC-B bridges (BR17-19) are presented in Figs. 16 and 17. The component fragility curves illustrate well the development of component damage. LS1 is initiated by the yielding of the piers, and also in LS2, spalling of the outer concrete layer of piers is more likely at lower intensities (assumed to be the important portion of the fragility curve). However, it seems that the shear resistance is still insufficient. Even for more flexible continuous girders, collapse is caused by the shear failure of the pier.

5.1.5. Composite I- and Box-Girder (COMP-I and COMP-B) Bridges

Similar behavior is observed in case of composite girders (Fig. 18), LS1 is initiated by the yielding of the piers, while collapse is caused by the insufficient pier shear resistance. The system fragility curves in Fig. 19 indicate that there are two composite box girders (BR24 and 25) that are clearly not designed for seismic loads, and that pier shear failure occurs

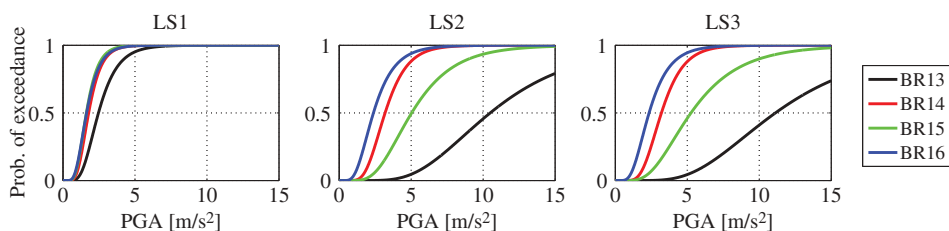


Figure 15. System fragility curves (full correlation in capacity) for SLAB bridges.

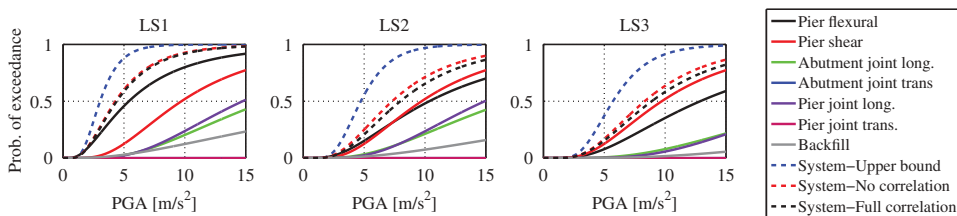


Figure 16. Fragility curves for the BR17 (RC-B) bridge.

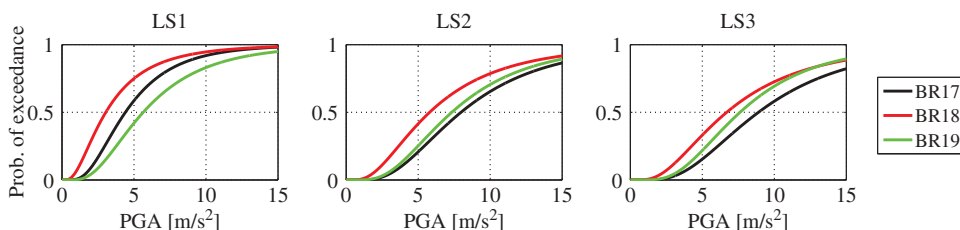


Figure 17. System fragility curves (full correlation in capacity) for RC-B bridges.

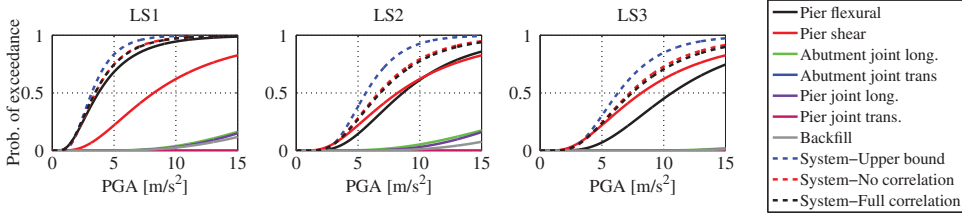


Figure 18. Fragility curves for the BR21 (COMP-I) bridge.

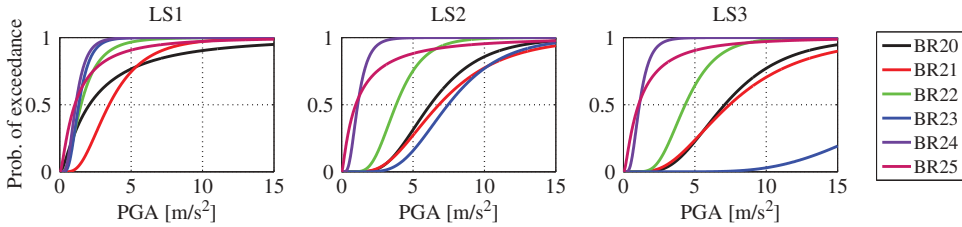


Figure 19. System fragility curves (full correlation in capacity) for COMP bridges.

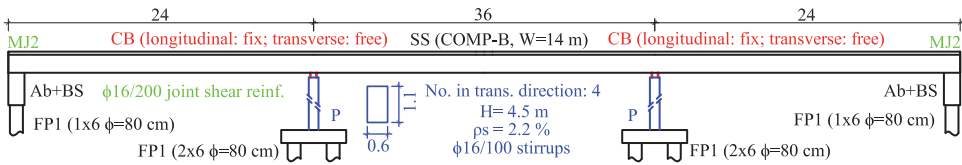


Figure 20. BR23 configuration with special bearing arrangement.

prior to any other component damage; therefore, the system fragility curves are identical to one another in all LSs.

The BR23 bridge should be highlighted due to its special configuration: monolithic MJ2 joints are used at the abutments, the piers are restrained in the longitudinal direction, while free movements can develop in the transverse direction (Fig. 20). Due to the supporting role of the abutment-backfill soil system, seismic pier demands are minimal in the longitudinal direction; besides, negligible horizontal forces are transferred to the pier by bearing friction in the transverse direction. Accordingly, the critical components are the abutment joints in LS1 and LS2, and it is also possible that failure is caused by unseating of the superstructure (see Abutment joint. trans. in Fig. 21). Note that the pier shear reinforcement is high ($\phi 16/100$ instead of the typical $\phi 12/150$), which—compared to the developing shear forces—indicates that pier shear failure is not expected. This configuration may be an economical solution for highway bridges with a total length up to 100 m.

5.1.6. Steel-I and Box-Girder (STEEL-I and STEEL-B) Bridges

Results for steel girders (BR26-30) are shown in Figs. 22 and 23. Figure 22 illustrates that steel bridges typically have an optimal behavior: pier flexural damage characterizes all three damage LSs, and energy dissipation due to the cyclic behavior of the piers can be utilized until collapse. Steel girder bridges are relatively flexible structures ($T_0 = 1.5-2$ s), large displacements are

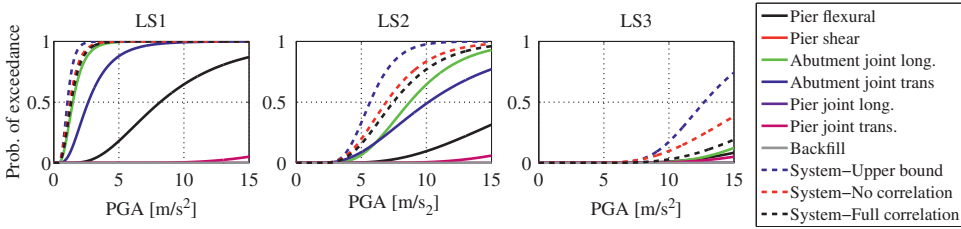


Figure 21. Fragility curves for the BR23 COMP-B bridge.

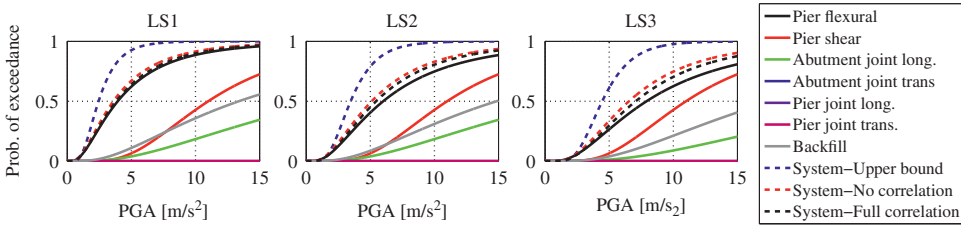


Figure 22. Fragility curves for the BR28 (STEEL-B) bridge.

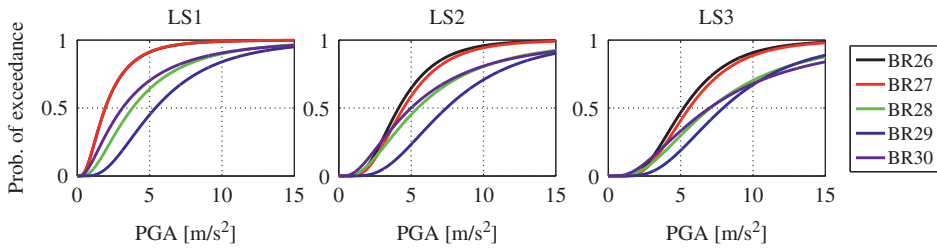


Figure 23. System fragility curves (full correlation in capacity) for STEEL bridges.

expected in case of an earthquake. However, Fig. 22 confirms that the developing longitudinal displacements are not large enough to cause unseating (measured with joint deformations), pier failure is always more likely to occur.

5.2. Reliability of the Structures

The β reliability index (Eq. (3)) for a 50-year reference period is calculated using the hazard curve for Komárom and Debrecen (area of highest and lowest seismicity in Hungary, see Fig. 4b) to provide a possible range of reliability levels in moderate seismic regions. The target reliability index is not unique and varies from code to code. EC0 specifies a target value only for Ultimate LS and Serviceability LS as 3.8 and 1.5, respectively, for structures with moderate consequences of failure (RC2 class). In the Joint Committee on Structural Safety Model Code [JCSS, 2001], it is proposed that the relative cost of safety measure (RCSM) should also be taken into account in the target reliability. It is stated that due to the large uncertainty in seismic loads, a lower reliability class should be used. Values of 1.98, 3.21, and 3.46 are

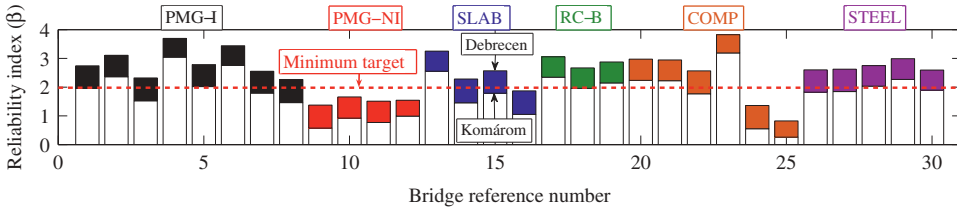


Figure 24. Range of reliability indices (β) related to collapse of the portfolio bridges (no correlation in capacity).

proposed for large, normal, and small RCSM, respectively; thus, a 1.98 target is adopted in this study to highlight structures that possibly need strengthening and retrofit.

The possible range of reliability indices for the portfolio bridges is presented in Fig. 24, where the upper and lower bounds are related to the area of Debreceen and Komárom, respectively. Reliability indices and the weakest components are also summarized for the Komárom area in Table 5. The reliability is highly dependent on many structural attributes (Table 2), thus only some concluding remarks can be made regarding the reliability of different structural types.

PMG-I bridges are critical (considering the area of Komárom) if the total length is over 80 m. Pier shear failure is dominant; however, 1500–2000 mm²/m pier shear reinforcement seems to be sufficient (see shear reinforcements in Table 2) to achieve the minimum target reliability except for the longest BR08 bridge with circular cross section ($D = 0.8$ m) and $\phi 10/100$ stirrups.

PMG-NI bridges perform worse, the calculated reliability index highlights the high vulnerability of these bridges, especially for shear failure. Some decrease of the base shear force can be achieved with this system due to the increased fundamental periods. However, this base shear force is distributed on fewer piers (for instance, BR12 is 8-span bridge, but it has only 2 longitudinally restrained supports in the middle), while in the transverse direction, these restrained piers carry the horizontal loads. Moreover, in case of the examined bridges, the applied shear reinforcement is even lower than in case of fully integrated PMG-I bridges.

Table 5. Calculated reliability indices (β) for Komárom (NC – no correlation; FC – full correlation in capacity). The weakest components: AJL, ABT – abutment joint longitudinal and transverse direction, respectively; SH – pier shear failure; FL – pier flexural failure).

Configuration		Weakest component			β (collapse)		Configuration		Weakest component			β (collapse)	
Class	BR	LS1	LS2	LS3	NC	FC	Class	BR	LS1	LS2	LS3	NC	FC
PMG-I	01	AJL	SH	SH	1.96	2.07	SLAB	16	AJL	SH	SH	1.05	1.26
	02	AJL	SH	SH	2.36	2.52		RC-B	17	FL	FL	SH	2.35
	03	AJL	SH	SH	1.52	1.82	18		FL	FL	SH	1.96	2.02
	04	AJL	AJL	FL	3.04	3.26	COMP-I	19	FL	SH	SH	2.15	2.26
	05	AJL	SH	SH	2.02	2.15		20	FL	FL	SH	2.24	2.26
	06	AJL	SH	SH	2.75	2.98		21	FL	SH	SH	2.22	2.22
	07	AJL	SH	SH	1.79	1.9		22	FL	FL	SH	1.77	1.85
	08	AJL	SH	SH	1.46	1.62	COMP-B	23	AJL	AJT	FL	3.19	3.44
PMG-NI	09	SH	SH	SH	0.57	0.86	24	SH	SH	SH	0.55	0.65	
	10	SH	SH	SH	0.92	1.13	25	SH	SH	SH	0.26	0.48	
	11	SH	SH	SH	0.77	0.99	STEEL-I	26	FL	FL	FL	1.82	1.95
	12	FL	SH	SH	0.99	1.51		27	FL	FL	FL	1.85	2.03
SLAB	13	AJL	SH	SH	2.55	2.69	STEEL-B	28	FL	FL	FL	2.03	2.09
	14	AJL	SH	SH	1.45	1.58		29	FL	SH	SH	2.27	2.31
	15	AJL	SH	SH	1.79	1.95		30	FL	FL	FL	1.89	1.97

Generally, some SLAB bridges perform considerably worse than PMG-I bridges. Shear failure is dominant, while the shear reinforcement is usually low (e.g. BR14 configuration has only $\phi 10/200$ stirrups). It is estimated that SLAB bridges would reach the minimal target reliability (even for Komárom) up to 80 m total length if a minimum of $\sim 2500 \text{ mm}^2/\text{m}$ pier shear reinforcement was applied.

Continuous girder bridges with CBs perform well, especially steel girders that are shown to behave in an optimal way suffering pier flexural damage with the highest probability in each damage LS. BR23 should be highlighted since it is already shown in the fragility analysis that the highest performance can be achieved with this bridge system and configuration. Focus should be laid on two composite box-girder bridges with 3 and 9 spans which are clearly not designed for seismic actions. Both configurations employ two circular piers in the transverse direction without tie beams and with low shear reinforcements ($\phi 16/200$ and $\phi 12/200$). The total length is 115 and 416 m for BR24 and BR25, respectively, while the number of restrained supports in the longitudinal direction is 1 and 2. This means that one pier supports half of the mass of 115 and 208 m superstructure. Moreover, torsion develops from the transverse vibration causing additional longitudinal shear forces in the pier pairs at the longitudinal restrained supports. This configuration is a typical example where mere strengthening is not a reasonable option, and the whole bridge behavior should be altered.

Figure 24 shows that the reliability index is highly dependent on the considered design site. The difference in the reliability index is 0.55–0.85, e.g., the β of the BR15 SLAB bridge is ~ 2.6 and ~ 1.9 if it is built in Komárom and Debrecen, respectively. Note that the bridge configuration is fixed (e.g. reinforcements, cross sections, capacities, etc.), and the results illustrate possible reliability indices of non-seismically designed bridges only.

Table 5 shows that a high portion of the examined bridges are highly susceptible to pier shear forces. To estimate what reliability level can be attained with seismic design according to EC8-2, the following procedure is carried out. An intensity-based evaluation using modal response spectrum analysis (MRSA) is conducted to calculate demand-capacity (DC) ratios associated with pier shear failure at the design PGA level (10% exceedance rate in 50 years) for all bridges. The standard shear resistance is computed per EC8-2. The last step is to assign the corresponding reliability indices to each configuration and then plot these β values against the DC ratios. The procedure is carried out for both areas, Komárom and Debrecen.

As confirmed by Fig. 25, the correlation between the reliability and the DC ratio can be described with a logarithmic function. The function does not depend on the actual site: the

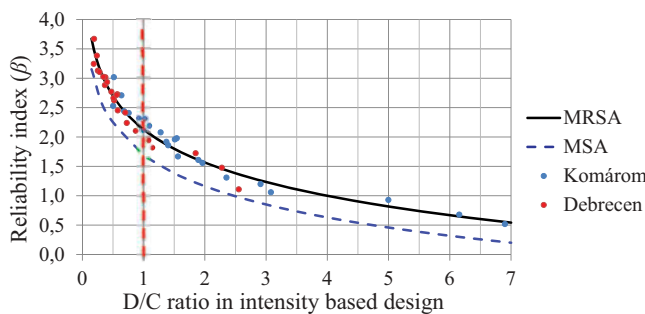


Figure 25. Reliability index against the DC ratios calculated at the design PGA level.

fitted curve represents well both Komárom and Debrecen. With seismic design ($DC \leq 1.0$), a reliability of index of ~ 2 or higher can be reached, which is in line with the minimum target reliability level proposed by JCSS. Note that an additional increase in the safety of the structure is introduced with the application of MRSA providing conservative estimates of seismic demands. For comparison, seismic demands are also calculated with a more rigorous approach using the median demands at the design PGA level determined during the MSA. The decreased demands lead to decreased DC ratios, and the fitted logarithmic curve is shifted to the left. In conclusion, if the bridge is designed for seismic demands calculated with more sophisticated methods, the reliability index may fall below 2.

The curve can also be used to estimate the required DC ratio for a specific β value. For instance, to reach a minimum target value of 2 with sophisticated analysis method, the DC ratio should be lower than 0.75 meaning that the piers should be overstrengthened by $\sim 30\%$. This additional factor may be incorporated in γ_{Bd} (applied to avoid brittle shear failure). Another option is to increase the return period and thusly the intensity of the design earthquake. In EC8-3, the return period of this earthquake is 2450 years for full collapse, while in case of new bridge design, the no-collapse criteria of EC8-2 specifies 475 years. This should be clarified and harmonized with the target reliability index for seismic loads. Moreover, the target reliability is also an open question. The determination of the target β should be based on rational economic calculations taking into account the consequences and the RCSM.

6. Conclusions

The seismic performance of several existing road bridges is questionable in many countries of moderate and low seismic zones due to the lack of proper seismic provisions. Therefore, it is an important issue to evaluate their seismic behavior to estimate the economic and financial consequences due to the developing damage caused by a seismic event. In this paper, fragility analysis and reliability assessment of 30 non-seismically designed bridges are conducted. The bridges are selected to represent typical bridges in a national bridge inventory. Detailed numerical models and hazard-consistent GMs are used for fragility analysis. Component fragility curves are created to analyze the damage mechanism of typical bridge types. Using the system fragility curves, the reliability indices of the structures are calculated to compare the seismic performance of representative bridge configurations.

Prior to the reliability assessment, preliminary studies are conducted related to the applied seismic load, modeling, and analysis assumptions. The following conclusions can be drawn from the preliminary study:

- The theoretical distribution of various GMIMs shows that the expected significant duration of GMs in Hungary (and probably in typical moderate seismic areas) is under 10 s, which is the minimum duration of the stationary part of the accelerograms according to EC8. Thus, considering the expected characteristics of possible earthquakes may lead to a decreased duration of the seismic load and less conservative seismic demands.
- Evaluation of different modeling and analysis assumptions on the seismic response shows the importance of modeling the cyclic behavior of monolithic joints and the pounding between bridge components. It is also shown that besides the uncertainty of the seismic load, the material and soil uncertainties may significantly influence the calculated probability of failure, while the geometric uncertainty is negligible.

On the basis of the reliability assessment results, the following concluding remarks can be made regarding the 30 specific examined configurations:

- The fragility analysis of the 30 examined configurations shows that the monolithic joints of integrated precast multi-girder and slab bridges are likely to suffer damage; while collapse is initiated by pier shear failure in most cases. Longer precast multi-girder bridges applying both EBs and monolithic joints are highly vulnerable, and pier shear failure occurs prior to any other component damage with high probability. Bridges with CBs have better behavior; however, collapse is related to insufficient pier shear resistance. More favorable ductile flexural failure is observed only in case of more flexible integral precast multi-girder and steel girder bridges.
- Comparing the reliability indices of the 30 bridges implies the better performance of integral precast multi-girder bridges and girder bridges with CBs, while typically certain slab bridges and longer precast multi-girder bridges with EBs have worse behavior.
- It is shown that a high reliability level can be achieved with a special configuration: with monolithic joints at the abutments, and conventional fix and free bearings in the longitudinal and transverse directions at the piers, respectively. This configuration is an optimal solution for highway overpass bridges up to 100 m total length.
- In certain cases, the calculated reliability level is extremely low (the β index for a 50-year reference period may fall below 1) due to the improperly chosen structural configuration and the lack of seismic design.
- The range of possible reliability indices of typical road bridges is presented in the paper. Since these bridges are not designed for seismic actions, the probability of collapse is highly dependent on the actual design site. A difference in the reliability index of 0.55–0.85 is observed considering two typical moderate seismic areas, the most and the least seismic area of Hungary.
- By comparing the intensity-based standard evaluation method to the reliability analysis results, it is shown that seismic design as per the Eurocode 8 standard leads to a reliability index of ~ 2 .

In conclusion, the insufficient pier shear resistance is a typical problem of several existing bridges in Hungary. The reliability indices highlight that numerous bridges do not reach the acceptable reliability level, indicating the necessity of retrofit measures in moderate seismic regions as well due to the lack of seismic design and inadequate detailing. The authors believe that the results can be useful in other moderate seismic areas since the paper provides a general illustration of the expected seismic performance and reliability levels of typical non-seismically designed road bridges.

Acknowledgments

The authors appreciate the help of the members of the Hungarian Transportation Administration for providing the raw data of the existing bridge database, and also the help of the members of Hungarian bridge design companies (Főmterv Zrt., MSc Mérnöki Tervező és Tanácsadó Kft., Speciálterv Építőmérnöki Kft., Uvaterv Zrt.) for the several consultations and for providing bridge plans and bridge data.

Funding

This paper was supported by the János Bolyai Research Scholarship of the Hungarian Academy of Sciences.

References

- Akkar, S. and Bommer, J. J. [2010] “Empirical Equations for the Prediction of PGA, PGV and Spectral Accelerations in Europe, the Mediterranean Region and the Middle East,” *Seismological Research Letters* **81**(2), 195–206, doi: [10.1785/gssrl.81.2.195](https://doi.org/10.1785/gssrl.81.2.195).
- Avşar, Ö., Yakut, A. and Caner, A. [2011] “Analytical fragility curves for ordinary highway bridges in Turkey,” *Earthquake Spectra* **27**(4), 971–996, doi: [10.1193/1.3651349](https://doi.org/10.1193/1.3651349).
- Baker, J. W. [2011] “Conditional Mean Spectrum: Tool for ground motion selection,” *Journal of Structural Engineering* **137**(3), 322–331, doi: [10.1061/\(ASCE\)ST.1943-541X.0000215](https://doi.org/10.1061/(ASCE)ST.1943-541X.0000215).
- Baker, J. W. [2015] “Efficient analytical fragility function fitting using dynamic structural analysis,” *Earthquake Spectra* **31**(1), 579–599. doi: [10.1193/021113EQS025M](https://doi.org/10.1193/021113EQS025M).
- Billah, A. H. M. M. and Alam, M. S. [2015] “Seismic fragility assessment of highway bridges: a state-of-the-art review,” *Structure and Infrastructure Engineering* **11**(6), 1–29. doi: [10.1080/15732479.2014.912243](https://doi.org/10.1080/15732479.2014.912243).
- Biskinis, D., Roupakias, G. and Fardis, M. N. [2004] “Degradation of shear strength of RC members with inelastic cyclic displacements,” *ACI Structural Journal* **101**(6), 773–783.
- Bommer, J. J. and Martinez-Pereira, A. [1999] “The effective duration of earthquake strong motion,” *Journal of Earthquake Engineering* **3**(2), 127–172.
- Bradley, B. A. [2010] “A generalized conditional intensity measure approach and holistic ground-motion selection,” *Earthquake Engineering and Structural Dynamics* **39**(12), 1321–1342. doi: [10.1002/eqe.995](https://doi.org/10.1002/eqe.995).
- Bradley, B. A. [2012a] “The seismic demand hazard and importance of the conditioning intensity measure,” *Earthquake Engineering and Structural Dynamics* **41**(11), 1417–1437, doi: [10.1002/eqe.2221](https://doi.org/10.1002/eqe.2221).
- Bradley, B. A. [2012b] “A ground motion selection algorithm based on the generalized conditional intensity measure approach,” *Soil Dynamics and Earthquake Engineering* **40**(1), 48–61, doi: [10.1016/j.soildyn.2012.04.007](https://doi.org/10.1016/j.soildyn.2012.04.007).
- Borzi, B., Ceresa, P., Franchin, P., Noto, F., Calvi, G. M. and Pinto, P. E. [2015] “Seismic vulnerability of the Italian roadway bridge stock,” *Earthquake Spectra* **31**(4), 2137–2161. doi: [10.1193/070413EQS190M](https://doi.org/10.1193/070413EQS190M).
- Campbell, K. W. and Bozorgnia, Y. [2010] “A ground motion prediction equation for the horizontal component of cumulative absolute velocity (CAV) based on the PEER-NGA strong motion database,” *Earthquake Spectra* **26**(3), 635–650.
- Caltrans. [2013] *Caltrans Seismic Design Criteria*. California Department of Transportation, Sacramento, CA, Version 1.7.
- CEN. [2005] MSZ EN 1337-3:2005. *Structural Bearings. Part 3: Elastomeric Bearings*.
- CEN. [2008a] MSZ EN 1998-1 Eurocode 8: *Design of Structures for Earthquake Resistance. Part 1: General Rules, Seismic Actions and Rules for Buildings*.
- CEN. [2008b] MSZ EN 1998-1 Eurocode 8: *Design of Structures for Earthquake Resistance. Part 2: Bridges*.
- CEN. [2009] MSZ EN 1998-5 Eurocode 8: *Design of Structures for Earthquake Resistance. Part 5: Foundations, Retaining Structures and Geotechnical Aspects*.
- CEN. [2011a] MSZ EN 1998-3 Eurocode 8: *Design of Structures for Earthquake Resistance. Part 3: Assessment and Retrofitting of Buildings*.
- CEN. [2011b] MSZ EN 1990-1 Eurocode 0: *Basis of Structural Design*.
- Chandramohan, R., Baker, J. W. and Deierlein, G. G. [2015] “Quantifying the influence of ground motion duration on structural collapse capacity using spectrally equivalent records,” *Earthquake Spectra* **32**(2), 927–950, doi: [10.1193/122813EQS298MR2](https://doi.org/10.1193/122813EQS298MR2).

- Dutta, A. [1999] "On energy based seismic analysis and design of highway bridges," Ph.D. thesis, State University of New York at Buffalo.
- Elnashai, A. S. and Di Sarno, L. [2008] *Fundamentals of Earthquake Engineering*, Wiley and Sons, UK.
- Fennema, J., Laman, J. and Linzell, D. [2005] "Predicted and measured response of an integral abutment bridge," *Journal of Bridge Engineering* **10**(6), 666–677, doi: 10.1061/(ASCE)1084-0702(2005)10:6(666).
- FIB. [2008] *Bulletin 43: Structural Connections for Precast Concrete Buildings*. International Federation for Structural Concrete.
- HTA. [2015] *Integrated Bridge Database*. Hungarian Transport Administration, Budapest, Hungary.
- Jalayer, F. and Cornell, C. A. [2009] "Alternative nonlinear demand estimation methods for probability-based seismic assessments," *Earthquake Engineering and Structural Dynamics* **38**(8), 951–972. doi: 10.1002/eqe.876
- Jayaram, N., Lin, T. and Baker, J. W. [2011] "A computationally efficient ground-motion selection algorithm for matching a target response spectrum mean and variance," *Earthquake Spectra* **27**(3), 797–815.
- JCSS [2001] Probabilistic Model Code. Zurich: Joint Committee on Structural Safety, ISBN 978-3-909386-79-6.
- Jernigan, J. B. and Hwang, H. [2002] "Development of bridge fragility curves," *7th US National Conference on Earthquake Engineering*, Boston, MA. EERI.
- Kibboua, A., Bechtoula, H., Mehani, Y. and Naili, M. [2014] "Vulnerability assessment of reinforced concrete bridge structures in Algiers using scenario earthquakes," *Bulletin of Earthquake Engineering* **12**(2), 807–827, doi: 10.1007/s10518-013-9523-7.
- Maroney, B. H. [1995] "Large scale bridge abutment tests to determine stiffness and ultimate strength under seismic loading," Ph.D. thesis, Dept. of Civil Engineering, University of California Davis, CA.
- McKenna, F., Scott, M. H. and Fenves, G. L. [2010] "Nonlinear finite-element analysis software architecture using object composition," *Journal of Computing in Civil Engineering* **24**(1), 97–105, doi: 10.1061/(ASCE)CP.1943-5487.0000002.
- Monteiro, R. [2016] "Sampling based numerical seismic assessment of continuous span RC bridges," *Engineering Structures* **118**, 407–420.
- Monteiro, R., Delgado, R. and Pinho, R. [2016a] "Probabilistic seismic assessment of RC bridges: Part I – Uncertainty models," *Structures* **5**, 258–273.
- Monteiro, R., Delgado, R. and Pinho, R. [2016b] "Probabilistic seismic assessment of RC bridges: Part II – Nonlinear demand prediction," *Structures* **5**, 274–283.
- Moschos, I. F., Kappos, A. J., Panetsos, P., Papadopoulos, V., Makarios, T. and Thanopoulos, P. [2009] "Seismic fragility curves for Greek bridges: Methodology and case studies," *Bulletin of Earthquake Engineering* **7**(2), 439–468, doi: 10.1007/s10518-008-9077-2.
- NIBS [1999] *Earthquake Loss Estimation Methodology: HAZUS99 (SR2). Technical Manual*, National Institute of Building Sciences, Federal Emergency Management Agency, Washington, DC.
- Nielson, B. G. [2005] "Analytical fragility curves for highway bridges in moderate seismic zones," Ph.D. thesis, School of Civil and Environmental Engineering, Georgia Institute of Technology.
- Nowak, A. S. and Collins, K. R. [2000] *Reliability of Structures*. The McGraw-Hill, Boston, MA.
- Padgett, J. E. and DesRoches, R. [2007] "Sensitivity of seismic response and fragility to parameter uncertainty," *Journal of Structural Engineering* **133**(12), 1710–1718.
- Padgett, J. E., DesRoches, R. and Nielson, E. [2010] "Regional seismic risk assessment of bridge network in Charleston, South Carolina," *Journal of Earthquake Engineering* **14**(6), 918–933.
- Pinto, P. E. and Franchin, P. [2010] "Issues in the upgrade of Italian highway structures," *Journal of Earthquake Engineering* **14**, 1221–1252.
- PEER [2015] *NGA-West2 Database: Shallow Crustal Earthquakes in Active Tectonic Regimes*. Pacific Earthquake Engineering Research Center, University of California, Berkeley, California.
- Priestley, M. J. N., Seible, F. and Calvi, G. M. [1996] *Seismic Design and Retrofit of Bridges*, John Wiley & Sons, Inc., New York, NY.

- Psycharis, N. I. and Mouzakis, P. H. [2012] "Shear resistance of pinned connections of precast members to monotonic and cyclic loading," *Engineering Structures* **41**(1), 413–427, doi: [10.1016/j.engstruct.2012.03.051](https://doi.org/10.1016/j.engstruct.2012.03.051).
- Sextos, A. G., Pitilakis, K. D. and Kappos, A. J. [2003a] "Inelastic dynamic analysis of RC bridges accounting for spatial variability of ground motion, site effects and soil–structure interaction phenomena. Part 1: Methodology and analytical tools," *Earthquake Engineering & Structural Dynamics* **32**, 607–627.
- Sextos, A. G., Pitilakis, K. D., and Kappos, A. J. [2003b] "Inelastic dynamic analysis of RC bridges accounting for spatial variability of ground motion, site effects and soil–structure interaction phenomena. Part 2: Parametric study," *Earthquake Engineering & Structural Dynamics* **32**, 629–652.
- Shamsabadi, A., Rollins, K. and Kapuskar, M. [2007] "Nonlinear soil–abutment–bridge structure interaction for seismic performance-based design," *Journal of Geotechnical and Geoenvironmental Engineering* **133**(6), 707–720, doi: [10.1061/\(ASCE\)1090-0241\(2007\)133:6\(707\)](https://doi.org/10.1061/(ASCE)1090-0241(2007)133:6(707)).
- Simon, J., Vigh, L. G., Horváth, A. and Pusztai, P. [2015] "Application and assessment of equivalent linear analysis method for conceptual seismic retrofit design of Háros M0 highway bridge," *Periodica Polytechnica* **59**(2), 109–122. doi: [10.3311/PPci.7860](https://doi.org/10.3311/PPci.7860).
- Simon, J. and Vigh, L. G. [2016] "Seismic fragility assessment of integral precast multi-span bridges in areas of moderate seismicity," *Bulletin of Earthquake Engineering*, (in press), doi: [10.1007/s10518-016-9947-y](https://doi.org/10.1007/s10518-016-9947-y).
- Timosidis, D., Megalooikonomou, K. G. and Pantazopoulou, S. J. [2015] "Monolithic reinforced concrete bridge joints under cyclic excitation," *Engineering Structures* **101**(1), 477–493, doi: [10.1016/j.engstruct.2015.08.004](https://doi.org/10.1016/j.engstruct.2015.08.004)
- Timosidis, D. and Pantazopoulou, S. J. [2009] "Analytical modeling of monolithic joints in concrete bridges," *Bulletin of Earthquake Engineering* **7**(2), 411–438, doi: [10.1007/s10518-008-9102-5](https://doi.org/10.1007/s10518-008-9102-5).
- ÚT [2004] *Útügyi Műszaki Előírás ÚT 2-3.401 Közúti hidak tervezése, Általános előírások*, Magyar Útügyi Társaság, (in Hungarian).
- Vamvatsikos, D. and Cornell, C. A. [2002] "Incremental dynamic analysis," *Earthquake Engineering and Structural Dynamics* **31**(3), 491–514, doi: [10.1002/eqe.141](https://doi.org/10.1002/eqe.141).
- Wolf, J. P. [1985] *Dynamic Soil–Structure Interaction*. Prentice-Hall, Inc., New Jersey.
- Zelaschi, C., Forcellini, D., De Angelis, G. and Monteiro, R. [2015] "Performance based earthquake engineering approach applied to bridges in a road network," *Proceedings of the 5th ECCOMAS Thematic Conference on Computational Methods in Structural Dynamics and Earthquake Engineering (COMPdyn)*, Crete, Greece, May 25–27.
- Zelaschi, C., Monteiro, R., Pinho, R. [2016] "Parametric characterization of RC bridges for seismic assessment purposes," *Structures* **7**, 14–24.
- Zsarnóczay, Á., Vigh, L. G. and Kollár, L. P. [2014] "Seismic performance of conventional girder bridges in moderate seismic regions," *Journal of Bridge Engineering* **19**(5), 9 p. Paper 04014001, doi: [10.1061/\(ASCE\)BE.1943-5592.0000536](https://doi.org/10.1061/(ASCE)BE.1943-5592.0000536).



Appendix A

Median capacity values for LS1-LS3 limit states are shown in Table A1 (CoV values are presented in Table 3). Further details about Bearing 1 and Bearing 2 associated with each bridge class is shown in Table A2.

Table A1. Median capacity values for LS1-LS3 damage limit states.

BR	Pier			Bearing 1 - deformation [m]						Bearing 2 - deformation [m]						Backfill					
	Shear [kN]			Flexural [%]			Longitudinal			Transverse			Longitudinal			Transverse			Deformation [m]		
	LS1	LS2	LS3	LS1	LS2	LS3	LS1	LS2	LS3	LS1	LS2	LS3	LS1	LS2	LS3	LS1	LS2	LS3	LS1	LS2	LS3
01	905	905	905	0.28	0.30	0.40	0.002	0.05	0.5	0.002	0.05	0.45	0.002	0.05	0.4	0.002	0.05	0.4	0.03	0.06	0.3
02	877	877	877	0.28	0.30	0.39	0.002	0.05	0.5	0.002	0.05	0.45	0.002	0.05	0.4	0.002	0.05	0.4	0.03	0.06	0.3
03	743	743	743	0.28	0.30	0.38	0.002	0.05	0.45	0.002	0.05	0.45	0.002	0.05	0.3	0.002	0.05	0.45	0.03	0.06	0.3
04	1295	1295	1295	0.28	0.30	0.38	0.002	0.05	0.5	0.002	0.05	0.45	0.002	0.05	0.3	0.002	0.05	0.45	0.03	0.06	0.3
05	800	800	800	0.28	0.30	0.36	0.002	0.05	0.55	0.002	0.05	0.55	0.002	0.05	0.3	0.002	0.05	0.45	0.03	0.06	0.3
06	781	781	781	0.28	0.30	0.36	0.002	0.05	0.5	0.002	0.05	0.5	0.002	0.05	0.3	0.002	0.05	0.45	0.03	0.06	0.3
07	658	658	658	0.28	0.30	0.37	0.002	0.05	0.5	0.002	0.05	0.3	0.002	0.05	0.3	0.002	0.05	0.45	0.03	0.06	0.3
08	872	872	872	0.28	0.30	0.47	0.002	0.05	0.45	0.002	0.05	0.6	0.002	0.05	0.4	0.002	0.05	0.4	0.03	0.06	0.3
09	1460	1460	1460	0.28	0.30	0.48	0.075	0.45	0.45	0.075	0.6	0.6	0.002	0.05	0.4	0.002	0.05	0.4	0.03	0.06	0.3
10	1178	1178	1178	0.28	0.30	0.39	0.075	0.45	0.45	0.075	0.6	0.6	0.002	0.05	0.4	0.002	0.05	0.4	0.03	0.06	0.3
11	2140	2140	2140	0.28	0.30	0.40	0.075	0.45	0.45	0.075	0.6	0.6	0.002	0.05	0.4	0.002	0.05	0.4	0.03	0.06	0.3
12	850	850	850	0.28	0.30	0.36	0.065	0.45	0.45	0.065	0.6	0.6	0.002	0.05	0.4	0.002	0.05	0.4	0.03	0.06	0.3
13	835	835	835	0.28	0.30	0.38	0.002	0.05	0.4	0.002	0.05	2.4	x	x	x	x	x	x	0.03	0.06	0.3
14	2800	2800	2800	0.28	0.30	0.38	0.002	0.05	0.5	0.002	0.05	2.5	x	x	x	x	x	x	0.03	0.06	0.3
15	745	745	745	0.28	0.30	0.38	0.002	0.05	0.5	0.002	0.05	4.3	x	x	x	x	x	x	0.03	0.06	0.3
16	635	635	635	0.28	0.30	0.39	0.002	0.05	0.5	0.002	0.05	3.25	x	x	x	x	x	x	0.03	0.06	0.3
17	11780	11780	11780	0.28	0.30	0.36	0.5	0.5	1	0.5	0.5	5.5	0.5	0.5	1	0.5	0.5	3	0.03	0.06	0.3
18	11800	11800	11800	0.28	0.30	0.39	0.5	0.5	1.4	0.5	0.5	7	0.5	0.5	1	0.5	0.5	2.5	0.03	0.06	0.3
19	12500	12500	12500	0.28	0.30	0.37	0.5	0.5	1	0.5	0.5	8.5	0.5	0.5	1.4	0.5	0.5	3	0.03	0.06	0.3
20	21100	21100	21100	0.28	0.30	0.37	0.5	0.5	0.9	0.5	0.5	7	0.5	0.5	0.9	0.5	0.5	4.5	0.03	0.06	0.3
21	92300	92300	92300	0.28	0.30	0.40	0.5	0.5	1.3	0.5	0.5	7	0.5	0.5	0.9	0.5	0.5	4	0.03	0.06	0.3
22	6300	6300	6300	0.28	0.30	0.37	0.5	0.5	0.5	0.5	0.5	5.5	0.5	0.5	0.6	0.5	0.5	1.2	0.03	0.06	0.3
23	2100	2100	2100	0.28	0.30	0.38	0.002	0.05	0.5	0.002	0.05	7	x	x	x	0.5	0.5	0.55	0.03	0.06	0.3
24	2950	2950	2950	0.28	0.30	0.38	0.5	0.5	0.5	0.5	0.5	7	0.5	0.5	0.8	0.5	0.5	0.8	0.03	0.06	0.3
25	1750	1750	1750	0.28	0.30	0.43	0.5	0.5	0.6	0.5	0.5	7	0.5	0.5	0.7	0.5	0.5	0.7	0.03	0.06	0.3
26	7700	7700	7700	0.28	0.30	0.37	0.5	0.5	0.6	0.5	0.5	7	0.5	0.5	0.6	0.5	0.5	1	0.03	0.06	0.3
27	7700	7700	7700	0.28	0.30	0.38	0.5	0.5	0.6	0.5	0.5	7	0.5	0.5	0.6	0.5	0.5	1	0.03	0.06	0.3
28	7350	7350	7350	0.28	0.30	0.38	0.5	0.5	0.6	0.5	0.5	7	0.5	0.5	0.6	0.5	0.5	1	0.03	0.06	0.3
29	33600	33600	33600	0.28	0.30	0.40	0.5	0.5	1	0.5	0.5	11	0.5	0.5	1.85	0.5	0.5	1.75	0.03	0.06	0.3
30	7250	7250	7250	0.28	0.30	0.39	0.5	0.5	1	0.5	0.5	7	0.5	0.5	0.75	0.5	0.5	1.75	0.03	0.06	0.3

Table A2. Explanation of Bearing 1 and Bearing 2 associated with different bridge classes.

Bridge class	Bearing 1	Bearing 2	BR
PMG-I	Monolithic joint Type 2 at the abutments	Monolithic joint Type 2 at the piers	1–8
PMG-NI	Elastomeric bearing at some piers and the abutments	Monolithic joint Type 2 at other piers	9–12
SLAB	Monolithic joint Type 1 at the abutments	Monolithic joint Type 2 at the piers	12–16
BR23	Monolithic joint Type 2 at the abutments	Conventional bearings at the piers	23
OTHER	Conventional bearings at the abutments	Conventional bearings at the piers	Other

Appendix B

Table B1. Fragility curve parameters for portfolio bridges: median (θ_{fr}) and dispersion (β_{fr}).

Correlation	LS1				LS2				LS3			
	No		Full		No		Full		No		Full	
BR	θ_{fr}	β_{fr}	θ_{fr}	β_{fr}	θ_{fr}	β_{fr}	θ_{fr}	β_{fr}	θ_{fr}	β_{fr}	θ_{fr}	β_{fr}
01	2.01	0.39	2.28	0.43	4.70	0.34	5.39	0.37	4.70	0.34	5.39	0.37
02	1.99	0.38	2.24	0.43	6.69	0.27	8.07	0.31	6.73	0.27	8.08	0.31
03	0.65	1.35	0.81	1.22	3.15	0.44	4.46	0.49	3.16	0.46	4.52	0.50
04	1.53	0.36	1.66	0.37	8.08	0.31	9.16	0.32	14.09	0.37	17.83	0.40
05	1.82	0.33	2.01	0.37	5.08	0.38	6.04	0.42	5.20	0.40	6.11	0.43
06	2.22	0.37	2.50	0.37	9.66	0.33	12.04	0.34	10.90	0.39	14.70	0.45
07	1.21	0.47	1.32	0.50	4.45	0.51	5.16	0.55	4.51	0.53	5.21	0.56
08	1.40	0.37	1.54	0.38	2.89	0.43	3.53	0.49	2.90	0.44	3.56	0.47
09	1.03	0.50	1.49	0.55	1.03	0.51	1.47	0.58	1.02	0.50	1.49	0.55
10	1.69	0.72	2.28	0.71	1.70	0.71	2.28	0.67	1.71	0.71	2.25	0.71
11	1.34	0.73	1.80	0.68	1.39	0.69	1.83	0.65	1.40	0.71	1.82	0.65
12	1.81	1.26	2.59	0.88	2.56	1.32	3.77	0.83	2.84	1.37	4.17	0.85
13	2.28	0.39	2.47	0.43	8.52	0.40	10.49	0.44	9.51	0.46	11.13	0.47
14	1.61	0.34	1.78	0.39	2.74	0.34	3.19	0.38	2.75	0.34	3.21	0.38
15	1.48	0.38	1.63	0.39	4.00	0.42	5.04	0.46	4.20	0.44	5.26	0.50
16	1.40	0.42	1.64	0.43	1.84	0.45	2.38	0.48	1.82	0.45	2.35	0.47
17	4.30	0.58	4.40	0.59	7.30	0.56	7.98	0.57	8.32	0.53	8.90	0.57
18	2.89	0.73	3.04	0.74	5.36	0.66	5.80	0.69	6.22	0.67	6.69	0.67
19	5.13	0.62	5.64	0.60	6.13	0.58	7.34	0.57	6.64	0.53	7.62	0.54
20	2.04	1.19	2.08	1.21	5.94	0.44	6.21	0.45	6.68	0.43	7.09	0.46
21	3.49	0.54	3.46	0.56	6.67	0.50	6.82	0.51	7.26	0.53	7.43	0.55
22	1.35	0.65	1.49	0.66	3.34	0.37	3.82	0.39	3.91	0.37	4.33	0.40
23	1.24	0.46	1.34	0.46	6.90	0.38	7.46	0.40	16.92	0.41	21.27	0.40
24	0.99	0.51	1.12	0.50	0.99	0.49	1.13	0.50	0.99	0.48	1.12	0.50
25	0.76	1.33	1.06	1.18	0.76	1.34	0.99	1.37	0.75	1.33	1.06	1.19
26	1.73	0.68	1.94	0.71	3.58	0.46	4.14	0.51	4.32	0.43	5.21	0.49
27	1.59	0.68	1.94	0.70	3.53	0.46	4.47	0.51	4.41	0.42	5.59	0.48
28	3.60	0.74	3.82	0.75	5.11	0.70	5.45	0.71	6.54	0.64	7.07	0.65
29	5.26	0.62	5.40	0.62	7.06	0.54	7.44	0.54	7.51	0.51	7.94	0.52
30	2.55	1.37	3.13	0.89	4.51	0.79	5.00	0.80	6.14	0.74	6.99	0.77